

# Effects of Balloon Overhang on Stented Arteries

R.M. Pulliam<sup>1</sup>, M.R. Hyre<sup>2</sup>, & J.C. Squire<sup>2</sup>

<sup>1</sup>*Department of Mechanical Engineering, Villanova University, U.S.A.*

<sup>2</sup>*Department of Mechanical Engineering, Virginia Military Institute, U.S.A.*

## Abstract

Balloons are typically sized 1–2 mm longer than endovascular stents, yet the effects of the degree of balloon overhang are unknown. In this study, a computational model capable of predicting balloon/stent/artery interactions and their effects on arterial stresses was developed to assess the effects of length mismatch on stent expansion characteristics and arterial stress. A 16mm long, 1mm unexpanded diameter, slotted tube stent was modeled and expanded using contact frictional elements by a symmetrically-placed, tapered 17mm and 18mm balloon within an artery model. ANSYS was used to perform the FEA. This model takes into account the multilinear elastic balloon expansion, non-linear plastic stent expansion, and the hyper-elastic arterial deformations. In this study, endflare was defined by stent diameter at proximal end with respect to stent diameter at the midpoint. Results from this study indicate that maximum arterial stress at balloon contact is approximately proportional to the degree of balloon overhang. A 100% increase in balloon overhang results in a 4% increase in maximum endflare and a 39% change in peak arterial stress. However, at the end of expansion, which is of most clinical importance, the increase in max endflare is 2% and the increase in maximum arterial stress is 93% at the balloon point of contact and 45% at the point of contact with the far proximal and distal ends of the stent.

*Keywords: stent, vascular injury, balloon, restenosis, finite element analysis*

## 1 Introduction

Advances in prosthetic science and engineering have spurred the rapid development of many new permanent implants such as arterial reinforcement grafts, venous filters, myocardial perforation-sealing clamshells, and stents that strengthen and scaffold the biliary duct, urethra, veins, and arteries. These devices are typically attached to a delivery catheter and threaded to the site of interest where they are expanded. The very nature of the remote delivery systems make the mechanical details of implantation difficult to ascertain, yet this is important to quantify since there may be a link between how the devices are emplaced and the body's acute and chronic response. Endovascular stents in particular are ideal devices to quantify these relationships because of the extreme levels of stress they impose and because of their ubiquity; more than one million are annually implanted in the U.S. alone [1].

These studies suggest an upper limit exists to the success of purely biomedical approaches for managing post-device implantation, and a return to examining the mechanical initiators of vascular injury that occur during implantation. A complete understanding of the manner that stents expand may thus lead to both a new understanding of the processes of vascular adaptation to implants and possibly to the design and development of less-injurious devices. Experimental data are indirect; stents are too thin to be fully radioopaque, and methods of bringing a camera to the stent, such as intravascular ultrasound, are blocked by the balloon that expands the stent during the critical moments of implantation. Post mortem examinations indicate that restenosis is paradoxically more severe in the parts of the artery immediately outside the stented region, and animal studies have shown an unusual pattern of endothelial cell denudation occurring at a regular pattern at the center of stent struts, a superficial injury that may be a marker for deep vascular injury [5]. These data are not explained by current finite element analyses of arterial stresses in a stent-expanded artery [6-9] because no finite element models included the expansion of a balloon catheter in the model of a plastically-deformed stent.

The inclusion of the balloon catheter in the stent expansion model is not trivial. The problem is highly non-linear and includes complex contact problems between the stent, balloon, and arterial wall. Additionally, the balloon properties change dramatically depending on whether it is fully or partially inflated.

## 2 Geometry

The numerical study was performed on a three-dimensional stent/balloon/artery geometry. In addition to the usual difficulties in modelling the mechanical behavior of soft tissue, the overall system response is highly nonlinear due to the large plastic/multilinear-elastic/hyperelastic deformations of the individual components. The component geometries and constitutive material models are described below.

### 2.1 Artery

The coronary artery modeled was 30mm in length, with an inside diameter of 2.8mm and thickness of 0.3mm. Average element size was about 0.5mm long with a thickness of 0.15 mm. This configuration yielded a total of 7,680 elements.

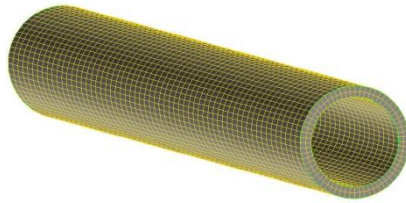


Figure 1: Artery Model

For finite element analysis in ANSYS, and the artery was assigned an element type of solid185. These elements are defined by eight nodes and are capable of large deflections and hyperelasticity

### 2.2 Balloon

The balloon was modeled in its unfolded state, and already assumed to be in contact with the stent. The balloon dimensions are given at 0 Pa, before stent expansion occurs. Depending on the amount of balloon overhang, the overall length of the balloon can range from 22-23 mm. For 1 mm balloon overhang, the total length of end balloon is 1 mm, or 0.5 mm on each side of the inside balloon, yielding a total balloon length of 22 mm. For 2 mm balloon overhang, the total length of balloon overhang is 2 mm, or 1 mm on each side, yielding a total balloon length of 23 mm (see fig. 2).

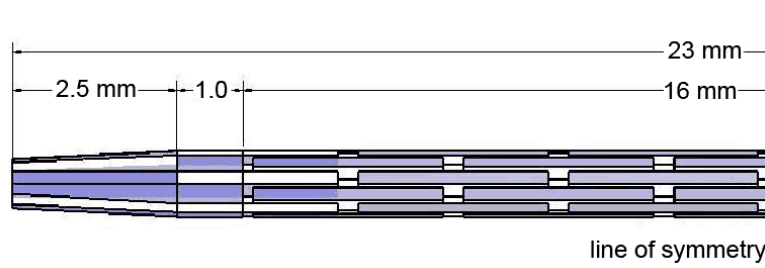


Figure 2: Balloon geometry, shown with mounted slotted tube stent.

The balloon was meshed using triangular shell elements with an average base size of 0.05 mm and an average side length of 0.05 mm. This yielded 54,456 elements for the 2 mm overhang case and 51,616 elements for the 1 mm overhang case (see fig. 3).

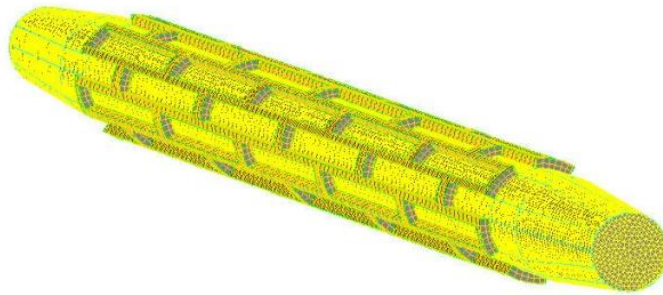


Figure 3: Balloon/Stent Mesh

For finite element analysis, an element type of shell43 was used for the balloon. These elements are capable of modeling shell structures and have large deflection and plasticity capabilities.

### 2.3 Stent

A three dimensional model of the slotted tube geometry intravascular stent was created. The stent is 16 mm in length (L), with an inside diameter (ID) of 1 mm, and a thickness (t) of 0.1 mm. The diamond-shaped stent consists of 5 slots in the longitudinal direction and 12 slots in the circumferential direction with length, l of 2.88 mm. The slots were cut such that in a cross-section, the angle describing the slot was approximately 23 degrees, and the angle describing the metal between slots was 6.9 degrees (See fig. 4 and 5). These dimensions refer to the model in an unexpanded state [7, 9].

The stent was meshed using hexahedral elements. There are 2 elements through the thickness of the stent yielding a total of 12,036 elements. The stent was assigned an element type of solid45 for finite element analysis in ANSYS. These elements are defined by eight nodes and are capable of large deflections and plasticity.

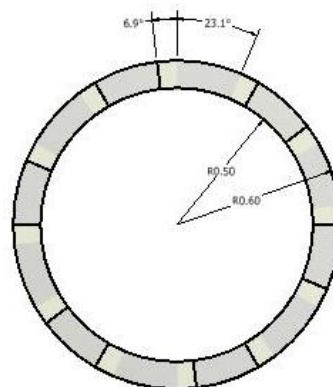


Figure 4: Medial Slice of Modeled Slotted Tube Stent

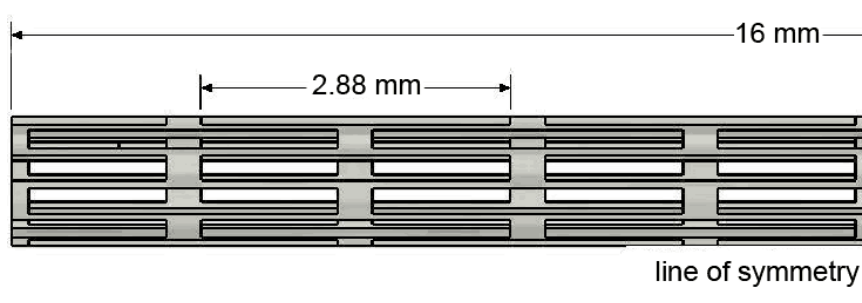


Figure 5: Side View of Modeled Slotted Tube Stent

### 3 Materials

#### 3.1 Artery

The material properties of the artery are based on a previous study by Lally *et al.* [9]. This model describes the behavior of the artery using a five parameter, third-order, Mooney-Rivlin hyperelastic constitutive equation. This model has been found to be suitable for modeling an incompressible isotropic material [10]. The final form of the strain density function used to model the artery is given in eqn. (1).

$$W = a_{10}(I_1 - 3) + a_{01}(I_2 - 3) + a_{20}(I_1 - 3)^2 + a_{11}(I_1 - 3)(I_2 - 3) + a_{30}(I_1 - 3)^3 \quad (1)$$

$W$  is the strain-energy density function of the hyperelastic material.  $I_1$ ,  $I_2$ , and  $I_3$  are the strain invariants.  $a_{ijk}$  are the hyperelastic constants. Lally *et al.* developed the constants for this model by fitting the five parameter Mooney-Rivlin expression to uniaxial and equibiaxial tension tests of human femoral arterial tissue data [11].

Hyperelastic Constants [Pa]
$a_{10} = 0.01890$
$a_{01} = 0.00275$
$a_{20} = 0.08572$
$a_{11} = 0.59043$
$a_{30} = 0$

#### 3.2 Balloon

To model the mechanical properties of the balloon without evaluating the balloon's behavior during unfolding, empirical data was used. The stress-strain curve for the full expansion of the balloon produced a linear piecewise function. The first segment of the piecewise function is representative of the unfolding

balloon, while the second is of the balloon expansion after unfolding. This accurately reproduced the balloon expansion dynamics while allowing significant reduction in the computational complexity of modeling the balloon unfolding process. The stress-strain curves used to model the properties of the balloon at different axial locations was developed from the balloon diameter vs. pressure curve which shown in Figure 6.

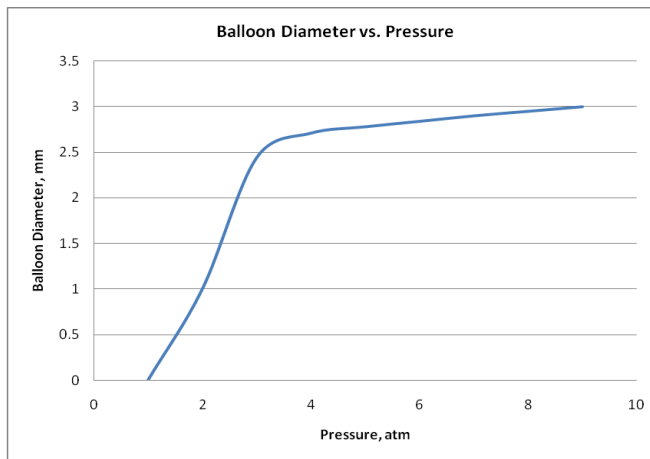


Figure 6: Balloon Stress/Strain Curves

### 3.3 Stent

The stent was modeled after the Palmaz-Schatz model given by Migliavacca *et al.* [7]. This model assumes the stent to be made of 316LN stainless steel. The Poisson ratio is 0.3 and the Young Modulus is 200 GPa. The stress-strain curve used to model the expansion of the stent is shown in figure 7.

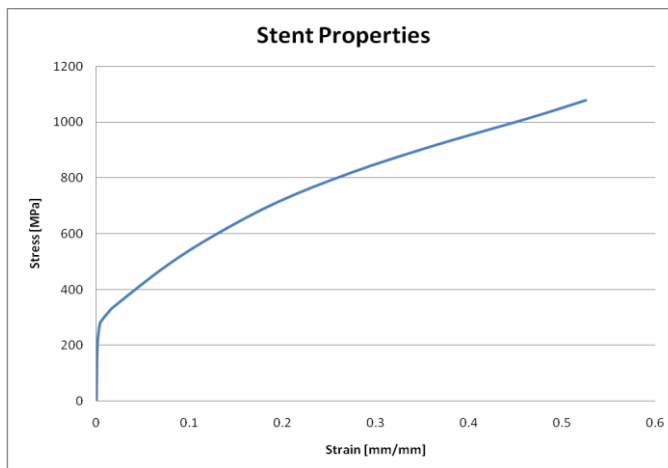


Figure 7: Stent Stress/Strain Curve

## 4 Boundary Conditions

The artery, balloon, and stent were all constrained in the rotational directions allowing no rotation. The artery was constrained axially at the distal ends. The artery was at a minimum, 7mm longer than the stent on each side and 3.5mm longer than the end of the balloon on each side. This constraint on the artery did not affect the behavior of the artery at the point of contact with the stent or balloon because of the extra length of the artery on both sides. The same axial constraint was placed on the balloon. To model the expansion of the balloon the balloon was assigned a ramped internal pressure load.

## 5 Results and Discussion

Figure 8 shows the endflare during stent expansion for the 1mm and 2mm balloon overhang cases. Endflare is defined as the ratio of the stent diameter at the distal ends to the diameter at the stent centerline. Figure 9 shows the condition of the stent/balloon/artery system at the points of maximum endflare. There is a dramatic difference in the endflare both at the point of peak endflare and at the end of expansion, indicating that the amount of balloon overhang can have a significant impact on vascular injury.

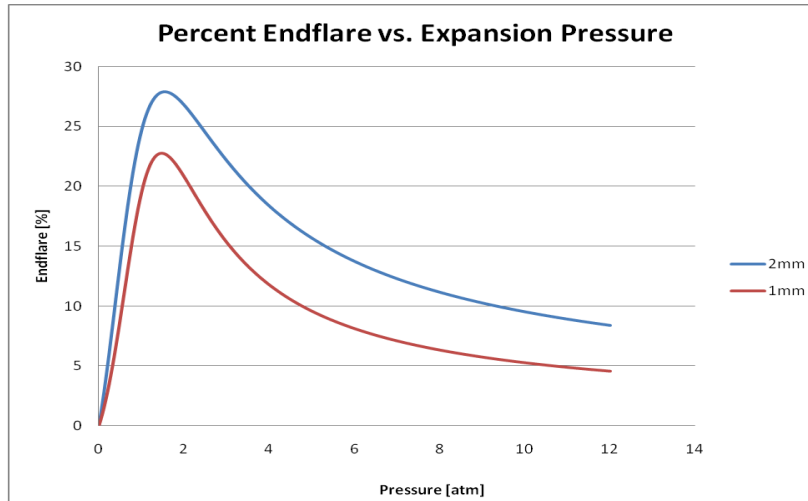


Figure 8: Percent Endflare for 1mm and 2mm Balloon Overhang Cases

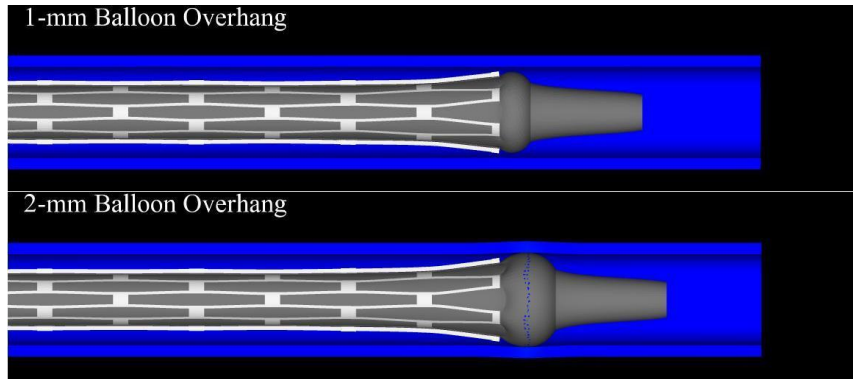


Figure 9: Stent/Balloon/Artery System at Point of Max Endflare

Figure 10 shows the arterial stresses at the end of stent expansion for both the 1mm and 2mm overhang cases. At the end of expansion, which is of most clinical importance, the increase in maximum endflare for the 2mm overhang geometry over the 1mm overhang geometry is 2%. The increase in maximum arterial stress is 93% at the point of balloon contact just beyond the far distal and proximal ends of the stent and 45% at the point of stent contact at the proximal and distal ends.

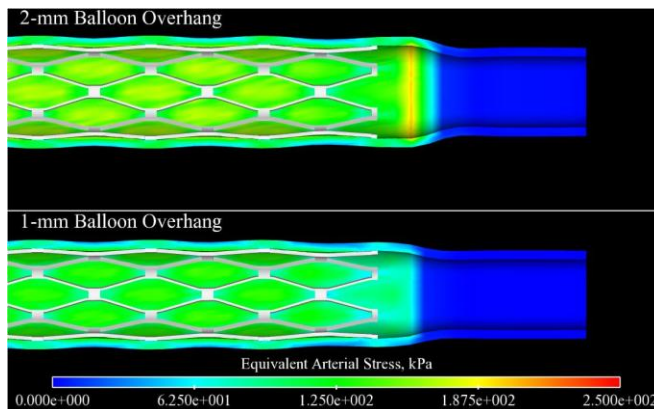


Figure 10: Arterial Stresses at the End of Stent Inflation

Figure 11 shows the amount of balloon/artery interaction during stent inflation. As one would expect, there is a significant increase in the area of balloon/artery contact of approximately 33 percent.

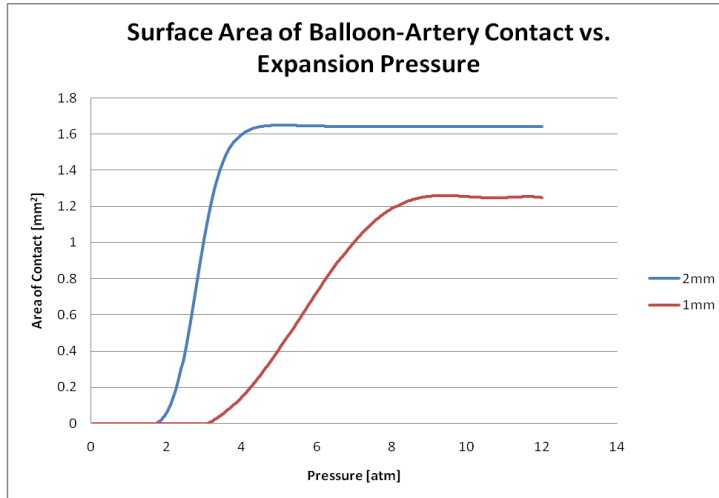


Figure 11: Comparison of Balloon/Artery Contact Areas

## 6 Clinical Significance of Report:

Concerns that drug-eluting stents interfere with the process of reendothelization and thus may encourage long-term thrombosis have spurred interest in understanding the mechanisms causing acute deendothelization during the stenting procedure. The effects of balloon overhang on resulting arterial stress is of particular interest because of discontinuities in standard overhang during stenting procedures. Yet, numerical instabilities caused by balloon unfolding and the extreme plastic distortion of the stent have previously prevented simulation of the balloon, stent, and artery using full-contact nonlinear algorithms. The methods presented in this paper allow the calculation of the luminal regions that are contacted by the balloon during stent implantation and thus denuded of endothelium. These methods may be applied to the design of drug-eluting stent geometries that preserve endothelium and so reduce risks of long-term thrombosis.

## References

- [1] Feder, Barnaby J, Panel Urges Caution on Coated Stents, New York Times - Health p1, Dec. 9 2006
- [2] Kuchulakanti PK, Chu WW, Torguson R, Ohlmann P, et al. Correlates and long-term outcomes of angiographically proven stent thrombosis with sirolimus- and paclitaxel-eluting stents. *Circulation*. 2006;113:1108 –1113.
- [3] McFadden EP, Stabile E, Regar E, Cheneau E, et al. Late thrombosis in drug-eluting coronary stents after discontinuation of antiplatelet therapy. *Lancet*. 2004;364:1519 –1521.
- [4] Ong AT, McFadden EP, Regar E, de Jaegere PP, van Domburg RT, Serruys PW. Late angiographic stent thrombosis events with drug eluting stents. *J Am Coll Cardiol*. 2005;45:2088 –2092.
- [5] Rogers C, Parikh S, Seifert P, Edelman ER. Endogenous cell seeding: Remnant endothelium after stenting enhances vascular repair. *Circ*. 1996; 11: 2909—2914.
- [6] F.Auricchio, M.Di Loreto, E.Sacco, Finite element analysis of a stenotic artery revascularization through stent insertion, *Computer Methods in Biomechanics and Biomedical Engineering* vol. 4, pg. 249-263, 2001
- [7] Migliavacca F, Petrini L, Colombo M et al. Mechanical behavior of coronary stents investigated through the finite element method. *Journal of Biomechanics* 2002; 35:803-811.
- [8] Petrini L, Migliavacca F, Dubini G, Auricchio F. Evaluation of intravascular stent flexibility by means of numerical analysis. 2003 Summer Bioengineering Conference, June 25-29, Key Biscayne, FL.
- [9] Lally, C., Dolan, Fl, and Prendergast, P.J., “Cardiovascular stent design and vessel stresses: a finite element analysis, *J. Biomechanics*, **38**, pp. 1574-1581, 2005.
- [10] Lally, C., Prendergast, P.J., 2003. An investigation into the applicability of a Mooney–Rivlin constitutive equation for modeling vascular tissue in cardiovascular stenting procedures. *Proceedings of the International Congress on Computational Biomechanics*. Zaragoza, Spain, pp. 542–550.
- [11] Prendergast, P.J., Lally, C., Daly, S., Reid, A.J., Lee, T.C., Quinn, D., Dolan, F., 2003. Analysis of prolapse in cardiovascular stents: a constitutive equation for vascular tissue and finite element modelling. *ASME Journal of Biomechanical Engineering* 125, 692–699.